Ab initio study of iron and iron hydride: III. Vibrational states of H isotopes in Fe, Cr and Ni

1998 J. Phys.: Condens. Matter 10 5131

(http://iopscience.iop.org/0953-8984/10/23/014)

J. Phys.: Condens. Matter **10** (1998) 5131–5146. Printed in the UK PII: S0953-8984(98)90980-8

Ab initio study of iron and iron hydride: III. Vibrational states of H isotopes in Fe, Cr and Ni

C Elsässer†‡‖, H Krimmel†, M Fähnle†, S G Louie‡ and C T Chan§¶

† Max-Planck-Institut für Metallforschung, Heisenbergstrasse 1, D-70569 Stuttgart, Germany
‡ Department of Physics, University of California, Berkeley, CA 94720, USA
§ Ames Laboratory and Department of Physics, Iowa State University, Ames, IA 50011, USA

Received 23 January 1998

Abstract. Adiabatic potentials, energy levels and wavefunctions for collective vibrational states of hydrogen isotopes in monohydrides of transition metals with face-centred cubic lattices, γ-FeH and NiH, and with body-centred cubic lattices, α-FeH and CrH, are investigated by means of *ab initio* total-energy calculations in the local density and local spin-density approximations (LDA, LSDA). The study for the different transition-metal monohydrides, including PdH and NbH studied earlier, yields a general insight into the microscopic vibrational potential wells: the topology of their spatial shapes is specific to the metal lattice, but their depths and curvatures change quantitatively in a systematic manner through the transition-metal series. The calculated excitation energies agree very well with results of inelastic neutron scattering (INS) experiments both for non-magnetic NiH, treated within the LDA, and ferromagnetic γ-FeH, treated within the LSDA. The theoretical data for the two considered hydrides, with bcc structure, for which corresponding experimental data do not exist, provide an *ab initio* database for the construction of metal–hydrogen interaction models, e.g., for studies of self-trapped vibrational states of isolated H atoms in transition metals.

1. Introduction

In this work, part III of our *ab initio* study of iron and iron hydrides (for parts I and II see references [1] and [2], respectively), we report theoretical investigations of the microscopic metal–hydrogen interactions in monohydrides of the first-row transition metals Cr, α-Fe, γ-Fe and Ni.

Experimental information about the metal–hydrogen interactions can be obtained by measuring lattice vibrations via inelastic neutron scattering (INS) [3–8]. Because of the large difference between the masses of metal and H atoms in transition-metal–hydrogen systems, the acoustic dispersion branches of the phonon spectra can be attributed to the motion of the metal atoms, the optic branches to the vibrations of the light H atoms relative to the metal lattice. The densities of states of optic phonons typically show a pronounced maximum at the energy of the lattice vibrations at the Γ point in the centre of the phonon Brillouin zone ($\boldsymbol{q} = 0$; cf., e.g., reference [3]). These phonon modes describe the vibration of the undistorted H sublattice relative to the rigid metal sublattice. Hence, they contain the metal–hydrogen interaction only. This is usually stronger than the H–H interaction, which

‖ Present address: Max-Planck-Institut für Metallforschung, Seestrasse 92, D-70174 Stuttgart, Germany.
¶ Present address: Physics Department, Hong Kong University of Science and Technology, Clear Water Bay, Hong Kong.

0953-8984/98/235131+16$19.50

leads to the dispersion of the optic branches. In the limit of very low H concentrations, the H vibrations can be imagined as independent vibrations of local Einstein oscillators at interstitial H sites.

For both the lattice vibrations at the Γ point and the local vibrations, one can observe transitions from the ground state, the quantum-mechanical zero-point vibration of the H atoms, to the first excited states, e.g. by measuring optic phonon excitations, and transitions to higher excited states. Their energies, intensities and symmetry splittings yield an insight into the shapes of the potential and the wavefunctions for the vibrations of the light particles.

Section 2 describes how the vibrational potentials and delocalized states in a periodic lattice are calculated. In sections 3 and 4 the results for H in the face-centred cubic (fcc) monohydrides NiH and γ-FeH and in the body-centred cubic (bcc) monohydrides α-FeH and CrH, respectively, are reported. Section 5 discusses the influence of a ferromagnetic spin polarization on the adiabatic potentials and vibrational energies.

2. Calculation of delocalized states

For the calculation of vibrational states of light particles in a rigid, heavy metal lattice the Born–Oppenheimer approximation can be applied twice. First, the electronic degrees of freedom are separated from both the hydrogen- and metal-ionic degrees of freedom. The quantum-mechanical ground state of the electrons for each spatial ionic configuration is determined using the local density-functional theory [9, 10] and the mixed-basis pseudopotential technique [11–13]. The ground-state total energies of the electron system form an adiabatic potential for the motions of the ion system. Second, the fast hydrogen motion, which leads to optic phonons, is separated from the slow metal-lattice motion, which is associated with the acoustic phonons. For the calculations for optic phonons, the heavy metal ions are assumed to be immobile.

The stoichiometric cubic transition-metal monohydrides are modelled as extended infinitely with three-dimensional translational periodicity. Then the undistorted crystals can be described by unit cells containing just one metal and one H atom, each unit cell with six motional degrees of freedom altogether (see appendix A). The three acoustic phonons at the Γ point simply correspond to three rigid-body translations of the whole crystal lattice. Hence their vibrational energies are zero. The three optic phonons at the Γ point, on the other hand, are characterized by an atomic displacement pattern where the one H ion in each unit cell is displaced relative to the one metal ion. In this case the adiabatic vibrational potential is a function of only the three degrees of freedom of the mutual displacements of the metal and hydrogen ions, thus forming a potential well in three dimensions, $V(\boldsymbol{r})$, where $\boldsymbol{r}$ is a displacement vector of the H atom away from its stable interstitial-lattice position (an octahedral or a tetrahedral site in the rigid fcc or bcc metal lattice, respectively; see below).

The energy E_ν and wavefunction $|\phi_\nu\rangle$ of a vibrational state (ν symbolizes a set of quantum numbers characterizing the state) are then obtained by solving the single-particle Schrödinger equation:

$$\left\{-\frac{\hbar^2}{2m_{\mathrm{H}}}\nabla_{\boldsymbol{r}}^2 + V(\boldsymbol{r})\right\}|\phi_\nu\rangle = E_\nu|\phi_\nu\rangle$$

with periodic boundary conditions ($V(\boldsymbol{r}) = V(\boldsymbol{r}+\boldsymbol{R})$, where $\boldsymbol{R}$ is a primitive translation vector of the crystal lattice; $\phi_\nu(\boldsymbol{r}) = \phi_\nu(\boldsymbol{r}+\boldsymbol{R})$ is a Bloch function for $\boldsymbol{q} = 0$). In the equation, the reduced mass μ is simply replaced by the nuclear mass of H, m_{H}, because this is much smaller than the mass of a transition-metal ion, and thus $\mu \approx m_{\mathrm{H}}$ (cf. appendix A). The one-particle Schrödinger equation is represented by a set of plane waves with kinetic

energies $|\boldsymbol{G}|^2 \leqslant E_{\mathrm{pw}}$ ($\boldsymbol{G}$ is a translation vector of the reciprocal lattice):

$$\sum_{G'} \left\{ \frac{\hbar^2}{2m_{\mathrm{H}}} |\boldsymbol{G}|^2 \delta_{G,G'} + V_{G-G'} \right\} \phi_{\nu G'} = E_\nu \phi_{\nu G}$$

where V_G and $\phi_{\nu G}$ are Fourier components of the adiabatic potential:

$$V(\boldsymbol{r}) = \sum_{G} V_G \mathrm{e}^{\mathrm{i}\boldsymbol{G}\cdot\boldsymbol{r}}$$

and of the wavefunction:

$$\phi_\nu(\boldsymbol{r}) = \sum_{G} \phi_{\nu G} \mathrm{e}^{\mathrm{i}\boldsymbol{G}\cdot\boldsymbol{r}}.$$

By exploiting the cubic symmetry of the crystals, the adiabatic potential can be written as a sum over symmetry-adapted linear combinations of plane waves (*star functions*):

$$V(\boldsymbol{r}) = \sum_{S} V_S \sum_{G_S} \mathrm{e}^{\mathrm{i}\boldsymbol{G}_S\cdot\boldsymbol{r}}$$

and by doing this the plane-wave matrix eigenvalue problem is transformed to a block-diagonal form with one block matrix for each irreducible representation. This reduces the effort required tremendously, because only the block matrices with dimensions of a few hundred star functions need to be diagonalized numerically instead of the whole matrix with a dimension of several tens of thousands of pure plane waves.

The diagonalizations yield Γ-point excitation energy spectra consisting of discrete energy levels E_ν. For a better comparison with measured INS spectra, a continuous density of states is formed by first referring all energies to the zero-point energy, $\varepsilon_\nu = E_\nu - E_0$, and second approximating δ-distributions by Gaussian functions of finite widths Δ_ν:

$$D(\varepsilon) = \sum_{\nu} \delta(\varepsilon - \varepsilon_\nu) \approx \sum_{\nu} \frac{1}{\Delta_\nu \sqrt{\pi}} \exp\left[\frac{\varepsilon - \varepsilon_\nu}{\Delta_\nu} \right]^2 .$$

As a measure for the width Δ_ν, experimental information like the relative resolution $\Delta_\nu/\varepsilon_\nu$ of an INS spectrometer can be used.

In the comparison of the theoretical vibrational densities of states with experimental INS spectra, it is important to be aware that the measured intensities are given approximately according to Fermi's golden rule as a product of the density of states and the transition probability which is given by matrix elements connecting initial- and final-state wavefunctions of the excitations. Such matrix elements, however, have been omitted in the present calculations. Hence only the energy positions of the lines in the DOS and the INS spectra can be compared, not their absolute or relative heights. This information, however, is already sufficient to determine the shape of the vibrational potential.

3. H in face-centred cubic NiH and γ-FeH

To determine the adiabatic potentials of these two monohydrides, first the equilibrium unit-cell volumes were calculated by minimizing the total energy as a function of the volume with H occupying all octahedral interstitial sites of the fcc metal lattice (NaCl structure). As described in part I, this was done by fitting the universal equation of state (EOS) of Rose *et al* [14] to the $E(V)$ data. The resulting theoretical equilibrium lattice constants for NiH and for γ-FeH are a_0(NiH) = 3.65 Å (experimental: 3.725 Å [15]) and a_0(γ-FeH) = 3.62 Å. For NiH it is natural to use the theoretical equilibrium lattice constant for the calculation of vibrational states, because this hydride can be stabilized at zero pressure (or atmospheric

pressure), e.g., by electric charging. For the close-packed FeH one can argue about whether a smaller lattice constant should be used, corresponding to a high external pressure at which this hydride is stable. Such a lattice constant for a given pressure can be found easily from the EOS presented in part II (see figures 2(b) and 3(b) there). However, because of the considerable differences in the calculated and measured bulk moduli (see table 2 in part II), which have a strong influence on the $p(V)$ curves, we consider the calculated $p(V)$ curves to be not sufficiently predictive to give a lattice constant related to a desired experimental value for the external pressure, which could be unambiguously preferred over the calculated zero-pressure value of the lattice constant. Specifically, for an external pressure of 3.6 GPa, above which the close-packed hydride FeH becomes stable in experiment, the corresponding lattice constants derived from the EOS are smaller than the zero-pressure lattice constant by 0.6% in the LDA and by 0.3% in the LSDA. Such subtle changes can lead to increases of the calculated vibrational energies by a few meV. However, since to our knowledge there is only one experimental result for such energies available to date [16], we think that in the present context a more extended theoretical discussion of the influence of pressure (or volume) on the vibrational H spectrum for FeH would be premature. Therefore all vibrational properties of FeH reported in the following were calculated using the theoretical equilibrium lattice constants at zero pressure.

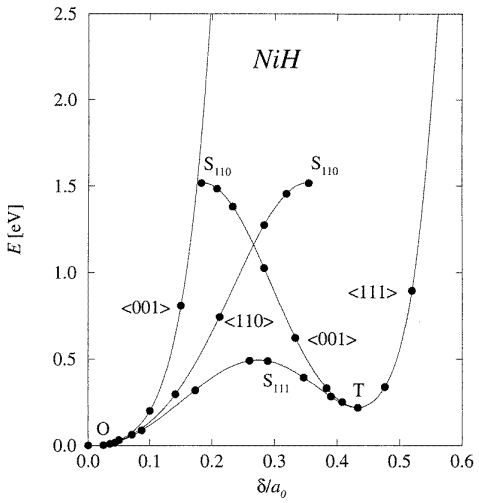

Figure 1. The adiabatic potential of H in NiH: the dependence of the total energy E on the position of H in a fcc unit cell with $a_0 = 3.65$ Å; for $\delta = 0$ the H atom is located at an O site. (The *ab initio* data points are marked by filled circles. The lines are cubic spline curves connecting the data points.)

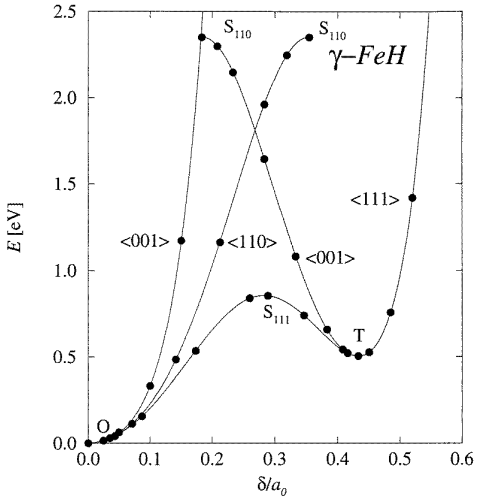

Figure 2. The adiabatic potential of H in γ-FeH: the dependence of the total energy E on the position of H in a fcc unit cell with $a_0 = 3.62$ Å; for $\delta = 0$ the H atom is located at an O site. (The *ab initio* data points are marked by filled circles. The lines are cubic spline curves connecting the data points.)

Next, for fixed unit-cell volumes and fixed positions of the metal atoms, the H sublattices were displaced out of the octahedral sites and the total-energy changes were monitored. The resulting *ab initio* data for the adiabatic potentials are given in the figures 1 and 2. Compared to our previously reported results for PdH [17] the potentials look qualitatively similar, but the steepness of the wells increases from PdH to NiH to γ-FeH. The change from PdH to NiH is mainly due to the smaller unit-cell volume of NiH (cf. a_0(PdH): theory: 4.07 Å [17]; experiment: 4.09 Å [18]). The change from NiH to γ-FeH is caused by a less efficient

screening of the ionic core charges by only eight valence electrons per Fe atom instead of ten per Ni or Pd atom. It can be shown [19] that the steepening of the potentials resulting from the reduction of the number of valence electrons from right to left along the transition-metal rows in the periodic table of elements is a very general behaviour and will also be seen for the bcc monohydrides in the next section.

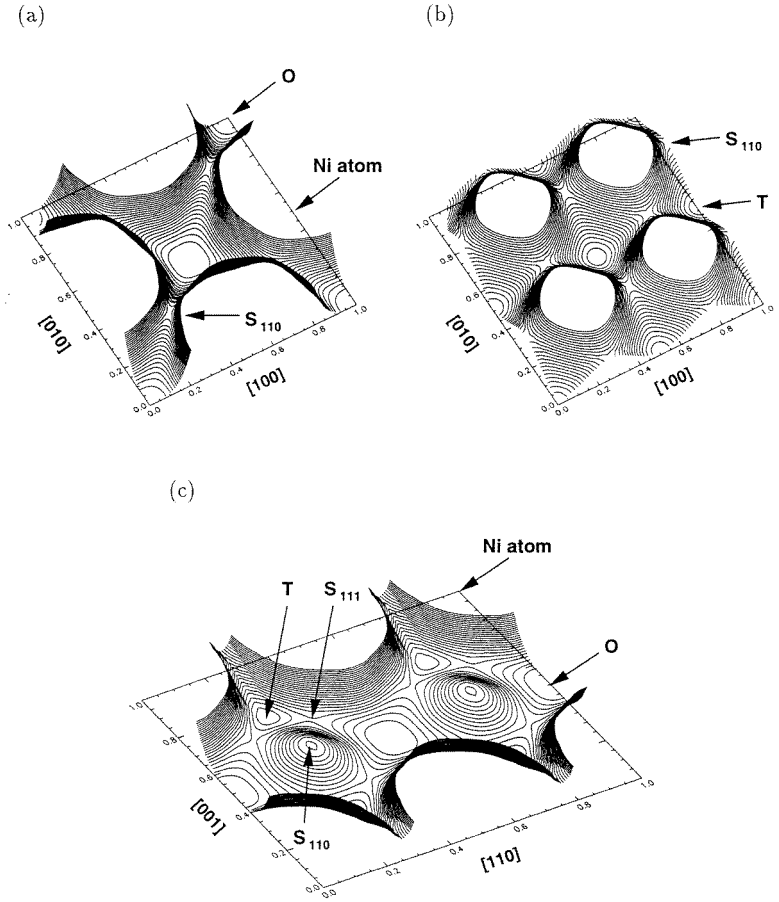

Figure 3. Constant-potential-energy contour plots of two-dimensional cuts through the three-dimensional adiabatic potential of H in fcc NiH: (a) an (001) plane passing through O sites (in the centre and at the corners) and Ni atoms (at the mid-points of the edges); (b) an (001) plane passing through T sites (in the centre, at the corners and at the mid-points of the edges); (c) a $(\bar{1}10)$ plane passing through O sites (in the centre and at the mid-points of the [001] edges), T sites (in the little triangular hollows) and Ni atoms (at the corners and at the mid-points of the [110] edges). (The energy difference between two neighbouring contour lines is 0.1 eV. The energy zero is at the O sites. The contour plots are cut off above a maximum energy of 2.5 eV.)

For the calculation of the vibrational energies, the adiabatic potentials are represented by a least-squares fit of 28 *ab initio* $E(V)$ data points to a Fourier series of 19 star functions ($|\boldsymbol{G}|^2 \leqslant 48(2\pi/a_0)^2$). (The potential fit parameters obtained, V_S, are listed in appendix B.) From these Fourier representations, the potentials can be obtained in real space via a discrete fast Fourier transformation and visualized by means of contour plots of two-dimensional cuts along selected crystal planes. Such contour plots for NiH are displayed in figure 3.

(Corresponding plots for γ-FeH look very similar.) In the cut through the octahedral sites (O sites) in an (001) plane (figure 3(a)) one sees the cubic anisotropy of the potential around the stable local minimum at the O sites and the steep ascent towards the Ni atoms due to the strong Ni–H interactions. The (001) cut through tetrahedral sites (T sites) (figure 3(b)) shows the metastable local minima with a noticeably less anisotropic well shape. The $(\bar{1}10)$ cut (figure 3(c)) passes through both O and T sites. It displays a low-energy classical-motion path from O to T to the next O along $\langle 111 \rangle$ directions, which was discussed in detail earlier for the case of PdH [17, 20, 21].

Table 1. Calculated zero-point energies $E_{0,|000\rangle}$ and excitation energies $\varepsilon_{\nu,|\nu\rangle}$ for vibrations of H isotopes in fcc NiH and γ-FeH (energies in meV; for the notation $|\nu\rangle$ for a state ν, see appendix 2 in reference [21]; the values in parentheses for protons are obtained by means of the potential scaling γ-FeH $\rightarrow$ NiH; see the text).

	NiH (LDA)					γ-FeH (LDA)			
	μ^+	p		d	t	μ^+	p	d	t
$E_{0,\|000\rangle}$	464	138	(136)	94	76	576	183	128	105
$\varepsilon_{1,\|100\rangle}$	331	99	(94)	68	54	398	124	86	70
$\varepsilon_{2,\|011\rangle}$		192	(178)	133	106		239	168	137
$\varepsilon_{2,\|C\rangle}$		208	(190)	142	113		252	175	142
$\varepsilon_{2,\|A\rangle} = \varepsilon_{2,\|B\rangle}$		221	(207)	148	116		269	183	147
$\varepsilon^{\mathrm{T}}_{0,\|000\rangle}$		335		304	290		623	590	575

The calculated results for the zero-point energies, E_0, and a few excitation energies, $\epsilon_\nu = E_\nu - E_0$, of Γ-point vibrations of H isotopes in NiH and γ-FeH are listed in table 1. Because of the cubic symmetry of the adiabatic potential there are singly, twofold- and threefold-degenerate states according to the irreducible representations of the point group O_h at the O sites. The ground state (zero-point state) belongs to Γ_1, corresponding to an atom-like s state or to a state $|nml\rangle = |000\rangle$ of a particle in a three-dimensional isotropic and harmonic potential well. The first excitation states are threefold degenerate (Γ_{15}, atom-like p states, oscillator states $|100\rangle$, $|010\rangle$ and $|001\rangle$). The second excitation states are threefold degenerate ($\Gamma_{25'}$, atom-like d states, oscillator states $|011\rangle$, $|101\rangle$ and $|110\rangle$). The next state is single (Γ_1, atom-like s state, oscillator state $|200\rangle + |020\rangle + |002\rangle$), and the following one is twofold degenerate (Γ_{12}, atom-like d states, oscillator states ($|200\rangle + |020\rangle - 2|002\rangle$, $|200\rangle - |020\rangle$)). The splitting of the latter six states with $n + m + l = 2$, which are all degenerate in the case of an isotropic and harmonic oscillator, are characteristic for the anisotropy and anharmonicity of the cubic potential well.

The line positions of the calculated excitation spectra for protons in NiH for which $n + m + l = 1$ and 2 can be compared directly to measured INS spectra [22–24]. For an illustration, the calculated DOS is plotted in figure 4(a) with a relative width $\Delta_\nu/\varepsilon_\nu = 5\%$. The positions of the lines of the optic phonons (first excitation at about 100 meV) and the second excitations (at about 200 meV) are in good agreement with the INS spectra of [24] and [22]. Like the INS spectrum of [24], the calculated DOS shows two maxima for the second excitations. However, as required by the cubic symmetry (representations $\Gamma_{25'}$, Γ_1 and Γ_{12}) and illustrated in the calculated DOS of figure 4(b), in which a smaller relative width of $\Delta_\nu/\varepsilon_\nu = 1\%$ was set, the DOS is composed of three superposed lines in this energy region.

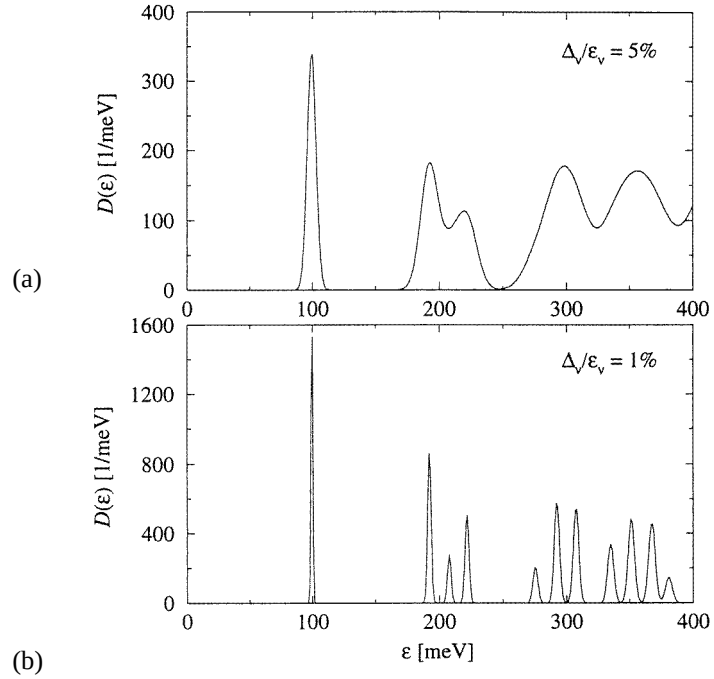

Figure 4. Densities of states obtained from the discrete excitation energies of Γ-point H vibrations in NiH using a Gaussian width of: (a) $\Delta_\nu/\varepsilon_\nu = 5\%$; (b) $\Delta_\nu/\varepsilon_\nu = 1\%$.

This feature is also apparent in PdH and has led us to a reinterpretation of the INS measurements from our earlier work [17]. Meanwhile, recent INS measurements on almost stoichiometric $PdH_{0.99}$ at a very low temperature $T = 15$ K [22] have come to our attention. In this measured INS spectrum (cf. figure 3 in reference [22]), besides the first line at 56 meV with the characteristic shoulder attributed to a dispersion of the optic phonon branches, there are three maxima clearly visible in the range from 100 meV to 150 meV, whose graphically estimated positions agree very well with our theoretically predicted excitation energies 117 meV, 132 meV and 147 meV, respectively, for protons in PdH [17]. Consequently, we are confident that the experimentally observed two-peak structure of the second excitation in NiH is also composed of three lines, which have just not been resolved experimentally. This relates to our concern [17] that important features of the potentials, which lead to line splittings, may be hidden and thus omitted in the assignment of INS line positions to excitation energies (cf., e.g., [25]; for an extensive discussion see [19]).

The corresponding theoretical zero-point and excitation energies of H isotopes in γ-FeH are not experimentally confirmed. However, there is strong evidence that close-packed FeH has some magnetic ordering [26–29]. We will address this point further in section 5 by studying the influence of a ferromagnetic spin polarization on the vibrational states.

4. H in body-centred cubic α-FeH and CrH

In this section, results of *ab initio* calculations for vibrational states of H isotopes in α-FeH and CrH are presented. Experimentally, both of these monohydrides are unstable, and Cr as well as α-Fe, as bcc metals, absorb H only in extremely low concentrations [15].

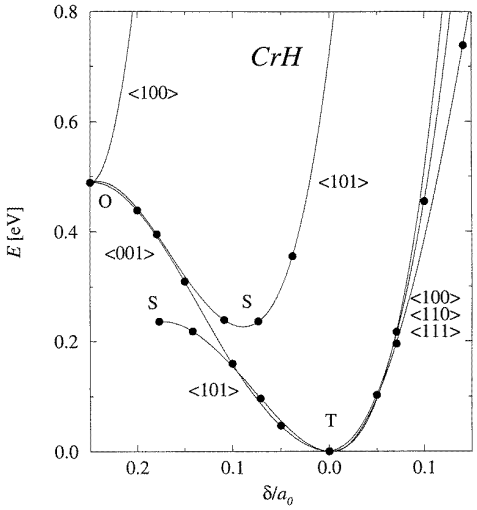

Figure 5. The adiabatic potential of H in CrH: the dependence of the total energy E on the position of H in a bcc unit cell with $a_0 = 3.04$ Å; for $\delta = 0$ the H atom is located at a T site. (The *ab initio* data points are marked by filled circles. The lines are cubic spline curves connecting the data points.)

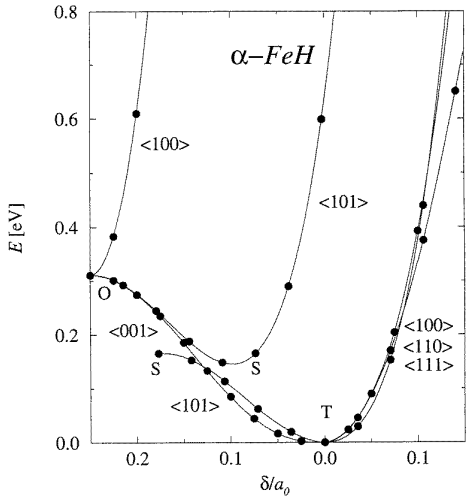

Figure 6. The adiabatic potential of H in α-FeH: the dependence of the total energy E on the position of H in a bcc unit cell with $a_0 = 2.96$ Å; for $\delta = 0$ the H atom is located at a T site. (The *ab initio* data points are marked by filled circles. The lines are cubic spline curves connecting the data points.)

Table 2. Calculated zero-point energies $E_{0,|000\rangle}$ and excitation energies $\varepsilon_{\nu,|\nu\rangle}$ for vibrations of H isotopes in bcc CrH and α-FeH (energies in meV; for the notation $|\nu\rangle$ for a state ν, see appendix 3 in reference [21]; the values in parentheses for protons are obtained by means of the potential scaling α-FeH $\rightarrow$ CrH; see the text).

	CrH (LDA)					α-FeH (LDA)			
	μ^+	p		d	t	μ^+	p	d	t
$E_{0,\|000\rangle}$	739	258	(249)	180	148	676	223	157	128
$\varepsilon_{1,\|001\rangle}$	344	112	(91)	84	71	305	81	58	47
$\varepsilon_{1,\|100\rangle} = \varepsilon_{1,\|010\rangle}$		168	(172)	126	105		150	113	96
$\varepsilon_{2,\|Q\rangle \approx \|002\rangle}$		205	(188)	159	136		170	120	99

Therefore the adiabatic potentials for the monohydrides shown in figures 5 and 6 and the resulting vibrational zero-point and excitation energies given in table 2 can be considered as theoretical results which are likely to be not directly checkable experimentally. Indirectly they have been very useful for the construction of an empirical metal–hydrogen interaction model for the study of vibrational states of isolated, single H atoms in metal lattices [30].

The adiabatic potentials were calculated again by first minimizing the total energy with respect to the unit-cell volume with H located at tetrahedral interstitial sites of the bcc metal lattice, yielding $a_0(\mathrm{CrH}) = 3.04$ Å and $a_0(\alpha\text{-FeH}) = 2.96$ Å. Second, for fixed volumes and fixed positions of the metal atoms, the energy changes due to displacements of the H sublattices were computed. The resulting potential parameters V_S of a Fourier representation with 21 star functions ($|\boldsymbol{G}|^2 \leqslant 36(2\pi/a_0)^2$) fitted to 26 *ab initio* $E(\delta)$ data points are listed in appendix B. The shape of the potential of α-FeH is illustrated by real-space contour plots in figure 7 (the potential for CrH has again a very similar shape).

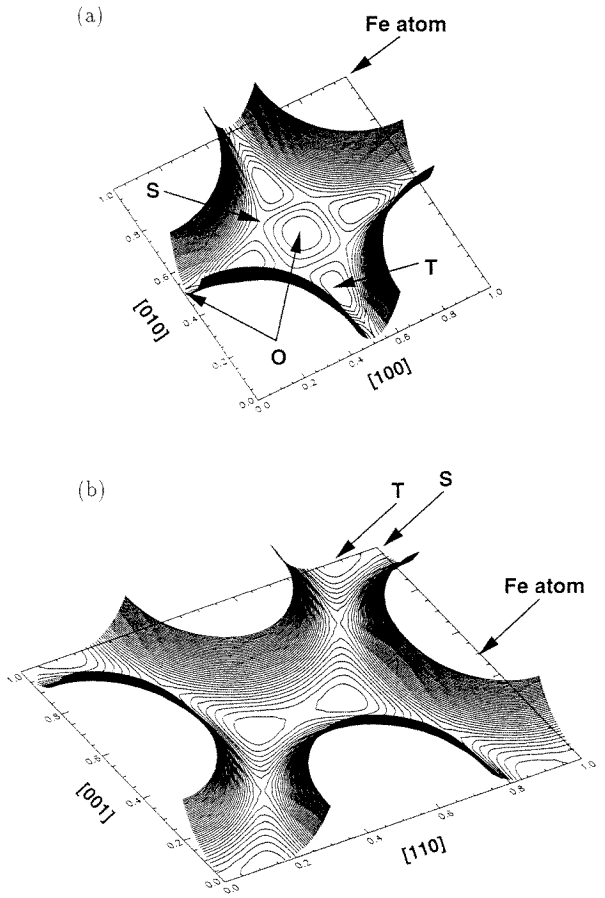

Figure 7. Constant-potential-energy contour plots of two-dimensional cuts through the three-dimensional adiabatic potential of H in bcc α-FeH: (a) an (001) plane passing through O sites (in the centre and at the mid-points of the edges), T sites (in four hollows surrounding the central O site) and Fe atoms (at the corners); (b) a $(\bar{1}10)$ plane passing through T sites (in triangular hollows close to the centre and the corners) and Fe atoms (at the mid-points of the edges). (The energy difference between two neighbouring contour lines is 0.05 eV. The energy zero is at the T sites. The contour plots are cut off above a maximum energy of 2.0 eV.)

Recent experiments with positive muons and pions, which can be considered as H isotopes with smaller nuclear masses ($m_{\mu^+}/m_{\mathrm{p}} = 1/9$, $m_{\pi^+}/m_{\mathrm{p}} = 1/7$), gave evidence that in Fe and Cr these light particles are probably located at interstitial octahedral (O) sites of the bcc lattices [31] instead of at tetrahedral (T) sites, where the ordinary isotopes p, d and t are commonly observed [32–34]. However, in the calculated adiabatic potentials for CrH and α-FeH (cf. figures 5 and 6), which have the translational periodicity of the crystal lattices, the stable local energy minima are obviously at T sites, and there are high-energy saddle points at O sites, like in the case of NbH [35, 21]. The periodic wavefunctions of vibrational states listed in table 2 are also concentrated at T sites. This is illustrated in figure 8 for the ground-state wavefunctions of μ^+ and p in α-FeH. For a visualization of the three-dimensional complex wavefunctions, cuts through their absolute squares, $|\phi^{\mu^+}_{\Gamma_1}(\boldsymbol{r})|^2$ and $|\phi^{\mathrm{p}}_{\Gamma_1}(\boldsymbol{r})|^2$, along (001) planes containing T sites of the bcc lattice are displayed as mesh

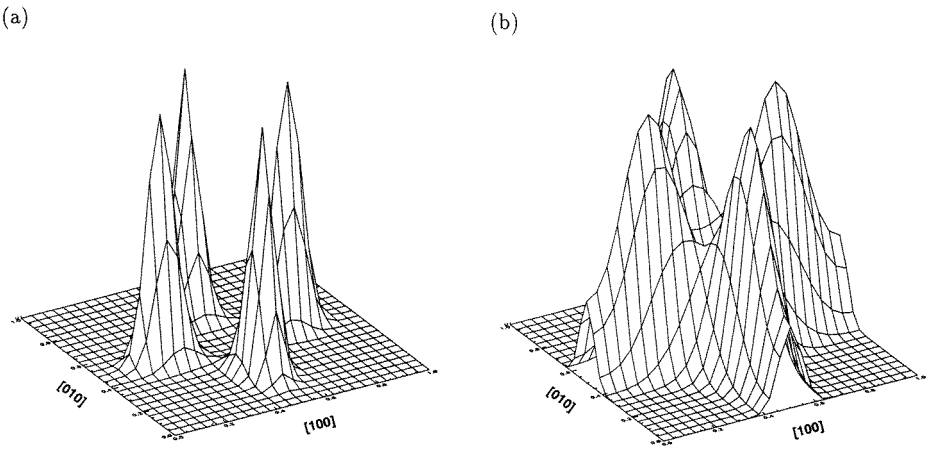

Figure 8. Mesh plots of two-dimensional cuts along cubic (001) planes through the absolute squares of the vibrational ground-state wavefunctions of H isotopes in bcc α-FeH: (a) $|\phi^{\mathrm{p}}_{\Gamma_1}(\boldsymbol{r})|^2$; (b) $|\phi^{\mu^+}_{\Gamma_1}(\boldsymbol{r})|^2$. (T sites are located below the maxima, O sites in the centre and at the mid-points of the edges, and Fe atoms at the corners.)

plots. Their maxima are located at T sites. While $|\phi^{\mathrm{p}}_{\Gamma_1}(\boldsymbol{r})|^2$ for the protons is strongly concentrated in the potential wells around T sites and almost decayed to zero in between, $|\phi^{\mu^+}_{\Gamma_1}(\boldsymbol{r})|^2$ for the muons is noticeably more distributed over the whole interstitial space. In particular its value at an O site is not negligible. This pronounced mass dependence of the shape and spatial distribution of wavefunctions leads further to an influence of the mass on the spatial shape of the adiabatic potential in the limit of very low H concentrations (see, e.g., chapter 4.6 in reference [3]). It finally results in the effect of self-trapping of the light particles by relaxations of the surrounding metal lattice and eventually to a mass dependence of the relative stability of occupied interstitial O or T sites. This effect was studied in detail in our previous work [30] for the case of H isotopes in α-Fe, where the *ab initio* data for the adiabatic potential of α-FeH reported above were used to construct an empirical two-body potential for the metal–hydrogen interaction. It was found that single positive muons and pions in bcc Fe do indeed occupy O sites whereas p, d and t occupy T sites. A corresponding investigation of self-trapping of H isotopes in bcc Cr and in fcc Ni, using the *ab initio* potential data of CrH and NiH shown in the figures 5 and 6, respectively, is documented in reference [19].

5. The influence of spin polarization

So far, all reported *ab initio* data for the adiabatic potentials were obtained by means of spin-unpolarized total-energy calculations in the local density approximation (LDA [10]). However, there is strong evidence that, like pure α-Fe, the recently synthesized close-packed high-pressure monohydride crystals ε-FeH are magnetically ordered, most probably ferromagnetically [26, 36]. Therefore it can be expected that the adiabatic potentials and the vibrational excitation energies of H are also influenced by the spontaneous bulk magnetization.

To study this influence of magnetism, spin-polarized total-energy calculations in the local spin-density approximation (LSDA, [37]) for both α-FeH and γ-FeH were performed.

First, the equilibrium lattice constants in the LSDA were calculated with H at the stable interstitial positions (T sites in bcc α-FeH, O sites in fcc γ-FeH): $a_0^{\mathrm{LSDA}}(\alpha\text{-FeH}) = 2.96$ Å, $a_0^{\mathrm{LSDA}}(\gamma\text{-FeH}) = 3.62$ Å.

The qualitative, topological shapes of the adiabatic potentials in bcc or fcc monohydrides throughout the whole transition-metal series are all the same. We found that quantitatively they can be scaled approximately with only two parameters by carrying out the following procedure in real space:

$$V(\boldsymbol{r}) \rightarrow V'(\boldsymbol{r}' = \alpha\boldsymbol{r}) = \beta V(\boldsymbol{r})$$

or in Fourier space:

$$V_{\boldsymbol{G}} \rightarrow V_{\boldsymbol{G}'=\boldsymbol{G}/\alpha} = \frac{\beta}{\alpha^3} V_{\boldsymbol{G}}$$

where the first scaling parameter is given by the ratio of equilibrium lattice constants, $\alpha = a_0'/a_0$, and the second one by an energy difference ΔE between H located at the interstitial site with lowest total energy (O site in γ-FeH; T site in α-FeH) and another characteristic interstitial H position (e.g., a T site or saddle point S_{111} in γ-FeH; an O site or saddle point S in α-FeH).

This scaling procedure was elaborated and justified in reference [19] for the potential scaling of PdH $\rightarrow$ $PdH_{0.25}$ and NbH $\rightarrow$ $NbH_{0.5}$. In these two cases it was found to be best if the energy differences ΔE were taken between O and S_{111} for the fcc hydrides, and between T and S for the bcc hydrides. From a comparison of the figures 1 with 2 and 5 with 6, respectively, it can be seen that the scaling also works reasonably well for γ-FeH $\rightarrow$ NiH ($\alpha = 1.009$, $\beta^{\mathrm{O-S_{111}}} = 0.571$) and for α-FeH $\rightarrow$ CrH ($\alpha = 1.026$, $\beta^{\mathrm{T-S}} = 1.426$), at least for the zero-point and first excitation energies. (Energies obtained from the scaled potentials of γ- and α-FeH are given in parentheses in tables 1 and 2, respectively, for comparison with NiH and CrH energies.) On the basis of this experience we assume the validity of this scaling procedure also for the transition LDA $\rightarrow$ LSDA for the iron monohydrides. The scaling parameters resulting from the LSDA–LDA differences in a_0 and in ΔE are

$$\alpha = \frac{a_0^{\mathrm{LSDA}}}{a_0^{\mathrm{LDA}}} = 1.017 \qquad \beta^{\mathrm{O-S_{111}}} = \frac{\Delta E^{\mathrm{LSDA}}}{\Delta E^{\mathrm{LDA}}} = 0.845 \qquad \beta^{\mathrm{O-T}} = 0.718$$

for fcc γ-FeH, and

$$\alpha = \frac{a_0^{\mathrm{LSDA}}}{a_0^{\mathrm{LDA}}} = 1.021 \qquad \beta^{\mathrm{T-S}} = \frac{\Delta E^{\mathrm{LSDA}}}{\Delta E^{\mathrm{LDA}}} = 1.031 \qquad \beta^{\mathrm{T-O}} = 1.175$$

for bcc α-FeH. Interestingly, the increases in a_0 caused by the spin polarization are similar for α-FeH and γ-FeH, whereas the changes in ΔE are opposite.

In the case of γ-FeH, the two scaling parameters together cause the potential to become flatter, which leads to a significant reduction of the vibrational energies, e.g., of $\varepsilon_{1,|100\rangle}$ for protons, by about 11% or 18% by scaling with $\beta^{\mathrm{O-S_{111}}}$ or $\beta^{\mathrm{O-T}}$, respectively. Hence, for a quantitative study of H vibrations in the close-packed γ-FeH it is essential to include the spin polarization. The resulting vibrational energies in the LSDA are listed in table 3. In particular, the energy of the first excitation of protons in γ-FeH, 102 meV for the scaling with $\beta^{\mathrm{O-T}}$ (this value was already given in reference [38]; see also [19]) or 110 meV for the scaling with $\beta^{\mathrm{O-S_{111}}}$, is very close to an energy loss of 105 meV reported from a very recent INS experiment on the close-packed high-pressure ε-FeH [16]. Since both the lattice spacings and neighbour coordinations around interstitial O sites are similar in the theoretically studied fcc γ-FeH and the experimentally studied dhcp ε-FeH, as demonstrated in part II, this is very strong evidence that the experimentally observed vibrational excitation

Table 3. Zero-point energies $E_{0,|000\rangle}$ and excitation energies $\varepsilon_{\nu,|\nu\rangle}$ for vibrations of H isotopes in spin-polarized fcc γ-FeH, as obtained by scaling the adiabatic potential of non-polarized fcc γ-FeH (energies in meV; the scaling parameters are given in the text; for the notation $|\nu\rangle$ for a state ν, see appendix 2 in reference [21]).

	γ-FeH (LSDA)							
	Scaling with $\beta^{O-S_{111}}$				Scaling with β^{O-T}			
	μ^+	p	d	t	μ^+	p	d	t
$E_{0,\|000\rangle}$	511	161	113	92	474	149	105	85
$\varepsilon_{1,\|100\rangle}$	352	110	76	62	326	102	71	57
$\varepsilon_{2,\|011\rangle}$		211	149	121		195	136	112
$\varepsilon_{2,\|C\rangle}$		224	155	125		207	144	116
$\varepsilon_{2,\|A\rangle} = \varepsilon_{2,\|B\rangle}$		240	163	130		223	151	121

Table 4. Zero-point energies $E_{0,|000\rangle}$ and excitation energies $\varepsilon_{\nu,|\nu\rangle}$ for vibrations of H isotopes in spin-polarized bcc α-FeH, as obtained by scaling the adiabatic potential of non-polarized bcc α-FeH (energies in meV; the scaling parameters are given in the text; for the notation $|\nu\rangle$ for a state ν, see appendix 3 in reference [21]).

	α-FeH (LSDA)							
	Scaling with β^{T-S}				Scaling with β^{T-O}			
	μ^+	p	d	t	μ^+	p	d	t
$E_{0,\|000\rangle}$	652	216	151	123	694	230	161	131
$\varepsilon_{1,\|001\rangle}$	324	78	56	46	327	83	60	49
$\varepsilon_{1,\|100\rangle} = \varepsilon_{1,\|010\rangle}$		144	109	93		156	118	100
$\varepsilon_{2,\|Q\rangle \approx \|002\rangle}$		164	115	95		174	124	102

[16] is the theoretically predicted transition from the ground state to the first excited state of protons in octahedral sites of the close-packed FeH.

In the case of α-FeH, the effects of the two parameters in the scaling almost cancel each other. ($\alpha > 1$ flattens but $\beta > 1$ steepens the potential.) Therefore the resulting vibrational energies in the LSDA, which are given in table 4, are not very different from those obtained in the LDA. This justifies the neglect of spin polarization in the investigation of self-trapped H states in α-Fe [30].

6. Summary

In this work, part III of our *ab initio* study of iron and iron hydrides, adiabatic potentials and vibrational states of H isotopes obtained from *ab initio* total-energy calculations using the mixed-basis pseudopotential method were reported for transition-metal monohydrides with fcc metal lattices, NiH and γ-FeH, and with bcc metal lattices, CrH and α-FeH. On comparing the results for several metal monohydrides, including the previously discussed fcc PdH and bcc NbH [17], it became clear that the topological shapes of the adiabatic potentials are characteristic for the metal-lattice types. With the reduction of the number of valence electrons (or ionic core charges) from right to left in the periodic table, the adiabatic

potentials become steeper and closer to harmonic and isotropic wells for the lowest few vibrational states.

While the ferromagnetism of pure Ni is suppressed in NiH [39], a ferromagnetic ordering, which was shown in parts I and II to remain stable in close-packed FeH, noticeably affects the interstitial H vibrations, as demonstrated by comparing LDA and LSDA calculations for fcc γ-FeH. The theoretically predicted first excitation energy for proton vibrations in spin-polarized fcc γ-FeH is quantitatively in accordance with the result of a recent INS experiment on the new high-pressure dhcp ε-FeH [16].

Acknowledgments

The present work was initiated during a research year for CE at the UC Berkeley. CE gratefully acknowledges the financial support of the Max Planck Society and the hospitality at Berkeley. This work was supported in part by the National Science Foundation (UC Berkeley: Grant No DMR-9520554) and the US Department of Energy (UC Berkeley: Contract No DE-AC03-76SF00098; Ames Laboratory: Contract No W-7405-ENG-82), including computer time at the NERSC in Livermore and the NCSA in Urbana–Champaign. CE, CTC and MF are grateful for the financial support of the NATO collaborative research grant No 910439. The valuable contributions of K-M Ho to the calculation technique for vibrational hydrogen states are gratefully acknowledged.

Appendix A. Normal-mode vibrations in cubic metal monohydrides

For the calculation of lattice vibrations for a selected wavevector $\boldsymbol{q}$ in the phonon Brillouin zone, the concept of *frozen lattice vibrations* is very suitable: first the displacement pattern of normal modes for the crystal considered are determined as irreducible representations by group-theoretical techniques (see, e.g., [40]). Second the total energy of the crystal is calculated, e.g., by the mixed-basis pseudopotential method, as a function of the amplitudes of atom displacements according to the normal-mode patterns. (This concept is often called the *frozen-phonon* method, but a harmonic approximation for the vibrational potential, which is fundamental for the quasiparticle concept of phonons, is not needed in the present context.)

The fcc monohydrides MH (NiH and γ-FeH) belong to the space group O_h^5 with 48 symmetry operations. The Bravais lattice is spanned by the vectors $\boldsymbol{a}_1 = (a/2)(011)$, $\boldsymbol{a}_2 = (a/2)(101)$ and $\boldsymbol{a}_3 = (a/2)(110)$. The two basis atoms are located at the equilibrium positions M (0, 0, 0) and H (1/2, 1/2, 1/2) with respect to the $\boldsymbol{a}_i$. The six-dimensional total representation D^{total} for the Γ point, $\boldsymbol{q} = 0$, can be reduced to two three-dimensional irreducible representations, $D^{\text{total}} = 2\Gamma_{15}$. One of them describes rigid translation modes of the whole crystal, i.e., in each of the three spatial directions both basis atoms are displaced by the same amplitude. A general rigid translation is a superposition of the three spatial displacements and corresponds to the acoustic Γ modes with zero excitation energy. The other irreducible representation is connected with normal modes, which are orthogonal to the translational modes. The two basis atoms are displaced in opposite directions with respect to each other. The amplitude of the H displacement is larger than that of the M displacement by a factor given by the nuclear mass ratio $m_{\text{M}}/m_{\text{H}}$. This distortion corresponds to the optic Γ modes.

The bcc monohydrides MH (CrH and α-FeH) belong to the tetragonal space group D_{2d}^9 with eight symmetry operations. The vectors $\boldsymbol{a}_1 = (a/2)(\bar{1}11)$, $\boldsymbol{a}_2 = (a/2)(1\bar{1}1)$ and

$\boldsymbol{a}_3 = (a/2)(11\bar{1})$ span the Bravais lattice. The equilibrium positions for the two basis atoms are M (0, 0, 0) and H (−1/4, 1/4, 1/2) with respect to the $\boldsymbol{a}_i$. The reduction of the six-dimensional total representation at the Γ point yields $D^{\text{total}} = 2\Gamma_4 + 2\Gamma_5$. One of the one-dimensional irreducible representations Γ_4 describes a rigid translation of the MH crystal in the z-direction (an acoustic mode with zero energy), the other one a relative displacement of the rigid M and H sublattices, again in the z-direction (an optic mode). Correspondingly, one of the two two-dimensional irreducible representations Γ_5 describes a superposition of rigid translations of the whole crystal in the x- and y-directions (acoustic modes with zero energies), the other one a superposition of the relative displacements of the two sublattices (optic modes).

Table A1. Fit parameters V_S of the Fourier representation of the adiabatic potentials for the Γ-point mode of H in fcc NiH ($a_0 = 3.65$ Å) and γ-FeH ($a_0 = 3.62$ Å) (energies in mRyd; 1 mRyd = 13.6058 meV; $\boldsymbol{G}$ denotes one of the plane waves composing one star function $\boldsymbol{G}_S$; a_0 is a calculated cubic equilibrium lattice constant).

$\boldsymbol{G}/(2\pi/a_0)$	V_S^{NiH}	$V_S^{\gamma-\text{FeH}}$
(0 0 0)	408.850	460.559
(1 1 1)	172.515	181.600
(0 0 2)	128.289	132.335
(0 2 2)	40.480	39.268
(1 1 3)	16.168	15.928
(2 2 2)	13.348	13.086
(0 0 4)	2.870	5.844
(1 3 3)	2.159	1.793
(0 2 4)	0.785	0.279
(2 2 4)	−0.357	−1.044
(3 3 3)	−0.201	−0.024
(1 1 5)	−0.274	−0.015
(0 4 4)	1.030	1.347
(1 3 5)	0.000	−0.320
(2 4 4)	0.157	0.522
(0 0 6)	0.862	2.559
(0 2 6)	−0.128	−0.372
(3 3 5)	−0.130	−0.116
(2 2 6)	−0.338	−0.915
(4 4 4)	−0.009	−0.120

Since the excitation energy of acoustic Γ vibrations is zero, the energies of optic Γ vibrations can be calculated also as a superposition of acoustic and optic modes where the heavy M sublattice is held fixed in space and the light H sublattice is displaced, thus being equivalent to 'a H vibration in a fixed M lattice'. Strictly, for the calculation of vibrational energies of particles in the adiabatic potential of a monohydride one should use the reduced masses accounting for both the H and M atoms instead of the nuclear mass of H alone. However, the mass of M is roughly 50 times larger than the mass of H, and the resulting difference between the H mass and the reduced mass is only 2% of the H mass and therefore negligible for the purposes of the present work.

In the ideal case of vibrations of light H particles in three-dimensional isotropic and harmonic potential wells, the energy change is independent of the direction and amplitude of the H displacement. Any dependence on direction or amplitude found in theory or experiment is a consequence of the anisotropy and the anharmonicity of the vibrational potential.

Table A2. Fit parameters V_S of the Fourier representation of the adiabatic potentials for the Γ-point mode of H in bcc CrH ($a_0 = 3.04$ Å) and α-FeH ($a_0 = 2.96$ Å) (energies in mRyd; 1 mRyd = 13.6058 meV; $\boldsymbol{G}$ denotes one of the plane waves composing one star function $\boldsymbol{G}_S$; a_0 is a calculated cubic equilibrium lattice constant).

$\boldsymbol{G}/(2\pi/a_0)$	V_S^{CrH}	$V_S^{\alpha-\mathrm{FeH}}$
(0 0 0)	610.532	581.059
(0 1 1)	267.064	259.832
(0 0 2)	115.709	113.586
($\bar{1}$ 1 2)	54.071	54.091
(0 2 2)	27.180	26.373
(0 1 3)	11.890	11.259
($\bar{2}$ 2 2)	6.321	6.717
($\bar{1}$ 2 3)	3.014	2.992
(0 0 4)	1.090	0.011
($\bar{1}$ 1 4)	0.003	0.014
(0 3 3)	1.161	0.662
(0 2 4)	−0.016	0.006
($\bar{2}$ 3 3)	−0.892	−0.005
($\bar{2}$ 2 4)	−0.601	0.202
($\bar{1}$ 3 4)	−0.125	0.009
(0 1 5)	0.140	−0.417
($\bar{1}$ 2 5)	−0.137	0.117
(0 4 4)	−0.256	−0.168
($\bar{3}$ 3 4)	−0.500	−0.322
(0 3 5)	−0.125	−0.043
($\bar{2}$ 4 4)	−0.043	−0.141
(0 0 6)	0.112	−0.370

For the cases of diluted H atoms in metals, the same displacement patterns of H relative to the M lattice also hold if the M lattice remains rigid and the local point symmetry at an occupied H site is retained.

Appendix B. Fourier representations of the adiabatic potentials

The fit parameters V_S of the Fourier expansion of the adiabatic potentials in the four transition-metal monohydrides considered in the present work are listed in tables A1 and A2.

Since the numbers of parameters V_S, which were determined by least-squares fits to *ab initio* $E(\delta)$ data, are rather large, the fit results are not unique. Equally good fits, i.e. which describe the potentials $V(\boldsymbol{r})$ comparably accurately, can be obtained using rather different parameter sets. The only complication that may happen is that artificial local minima can appear in spatial regions close to the metal atoms. These can be avoided by adding a few $E(\delta)$ data points for very small M–H distances with very high values well above the energy region relevant for the H vibrations. These do not affect the adiabatic potential and the vibrational states in the relevant energy ranges and space regions [19].

References

[1] Elsässer C, Zhu J, Louie S G, Fähnle M and Chan C T 1998 *J. Phys.: Condens. Matter* **10** 5081
[2] Elsässer C, Zhu J, Louie S G, Meyer B, Fähnle M and Chan C T 1998 *J. Phys.: Condens. Matter* **10** 5113
[3] Fukai Y 1993 *The Metal–Hydrogen System* (Berlin: Springer)

[4] Hunt D G and Ross D K 1976 *J. Less-Common Met.* **49** 169
[5] Springer T 1978 *Hydrogen in Metals I* ed G Alefeld and J Völkl (Berlin: Springer) ch 4
[6] Hempelmann R 1986 *Habilitationsschrift* RWTH Aachen (Berichte der Kernforschungsanlage Jülich No 2096)
[7] Hempelmann R 1987 *Z. Phys. Chem., NF* **154** 221
[8] Richter D, Hempelmann R and Bowman R C Jr 1992 *Hydrogen in Intermetallic Compounds II* ed L Schlapbach (Berlin: Springer) ch 3
[9] Hohenberg P and Kohn W 1964 *Phys. Rev.* **136** B864
[10] Kohn W and Sham L J 1965 *Phys. Rev.* **140** A1133
[11] Louie S G, Ho K-M and Cohen M L 1979 *Phys. Rev.* B **19** 1774
[12] Fu C-L and Ho K-M 1983 *Phys. Rev.* B **28** 5480
[13] Elsässer C, Takeuchi N, Ho K M, Chan C T, Braun P and Fähnle M 1990 *J. Phys.: Condens. Matter* **2** 4371
[14] Rose J H, Smith J R, Guinea F and Ferrante J 1984 *Phys. Rev.* B **29** 2963
[15] Fromm E and Gebhardt E (ed) 1976 *Gase und Kohlenstoff in Metallen* (Berlin: Springer)
[16] Cornell K, Wipf H, Kolesnikov A I, Antonov V E and Antonova T E 1997 *Verh. Deutsch. Phys. Ges.* **32** 839
[17] Elsässer C, Ho K M, Chan C T and Fähnle M 1991 *Phys. Rev.* B **44** 10 377
[18] Peisl H 1978 *Hydrogen in Metals I* ed G Alefeld G and J Völkl (Berlin: Springer) ch 3
[19] Elsässer C 1994 Ab-initio-Elektronentheorie für Übergangsmetall-Wasserstoff-Verbindungen *Habilitationsschrift* Universität Stuttgart
[20] Elsässer C, Fähnle M, Ho K M and Chan C T 1991 *Physica* B **172** 217
[21] Elsässer C, Ho K M, Chan C T and Fähnle M 1992 *J. Phys.: Condens. Matter* **4** 5207
[22] Kolesnikov A I, Natkaniec I, Antonov V E, Belash I T, Fedotov V K, Krawczyk J, Mayer J and Ponyatovsky E G 1991 *Physica* B **174** 257
[23] Eckert J, Majkzrak C F, Passell L and Daniels W B 1984 *Phys. Rev.* B **29** 3700
[24] Dorner B, Belash I T, Bokhenkov E L, Ponyatovsky E G, Antonov V E and Pronina L N 1989 *Solid State Commun.* **69** 121
[25] Rush J J, Rowe J M and Richter D 1984 *Z. Phys.* B **55** 283
[26] Ponyatovskii E G, Antonov V E and Belash I T 1982 *Sov. Phys.–Usp.* **25** 596
[27] Murayama H 1986 *J. Phys. Soc. Japan* **55** 2834
[28] Tsunoda Y, Imada S and Kunitami N 1988 *J. Phys. F: Met. Phys.* **18** 1421
[29] Tsunoda Y 1989 *J. Phys.: Condens. Matter* **1** 10 427
[30] Krimmel H, Schimmele L, Elsässer C and Fähnle M 1994 *J. Phys.: Condens. Matter* **6** 7705
[31] Seeger A and Schimmele L 1992 *Perspectives of Meson Science* ed T Yamazaki, K Nakai and K Nagamine (Amsterdam: Elsevier) p 293
[32] Carstanjen H D 1980 *Phys. Status Solidi* a **59** 11
[33] Carstanjen H D 1989 *Z. Phys. Chem., NF* **165** 141
[34] Ligeon E, Danielou R, Fontenille J and Eymery R 1986 *J. Appl. Phys.* **59** 108
[35] Tao H-J, Ho K-M and Zhu X-Y 1986 *Phys. Rev.* B **34** 8394
[36] Choe I, Ingalls R, Brown J M, Sato-Sorensen Y and Mills R 1991 *Phys. Rev.* B **44** 1
[37] von Barth U and Hedin L 1972 *J. Phys. C: Solid State Phys.* **5** 1629
[38] Elsässer C, Fähnle M, Ho K M, Chan C T and Louie S G 1994 *Verh. Deutsch. Phys. Ges.* **29** 1314
[39] Vargas P and Christensen N E 1987 *Phys. Rev.* B **35** 1993
[40] Inui T, Tanabe Y and Onodera Y 1990 *Group Theory and Its Applications in Physics* (Berlin: Springer)